Fluorescent probes for super-resolution imaging in living cells

Marta Fernández-Suárez[*‡] *and Alice Y. Ting*[*]

Abstract | In 1873, Ernst Abbe discovered that features closer than ~200 nm cannot be resolved by lens-based light microscopy. In recent years, however, several new far-field super-resolution imaging techniques have broken this diffraction limit, producing, for example, video-rate movies of synaptic vesicles in living neurons with 62 nm spatial resolution. Current research is focused on further improving spatial resolution in an effort to reach the goal of video-rate imaging of live cells with molecular (1–5 nm) resolution. Here, we describe the contributions of fluorescent probes to far-field super-resolution imaging, focusing on fluorescent proteins and organic small-molecule fluorophores. We describe the features of existing super-resolution fluorophores and highlight areas of importance for future research and development.

Electron microscopy
A focused electron beam is used to illuminate the sample. Electron microscopes use electrostatic and electromagnetic lenses to form the image by focusing the electron beam in a manner that is similar to how a light microscope uses glass lenses to focus light.

[*]*Department of Chemistry, Massachusetts Institute of Technology, 77 Massachusetts Avenue, Cambridge, Massachusetts 02139, USA.*
[‡]*Center for Engineering in Medicine, Massachusetts General Hospital, 114 16th Street, Charlestown, Massachusetts 02129, USA.*
e-mails: martafs@alum.mit.edu; ating@mit.edu
doi:10.1038/nrm2531
Published online
12 November 2008

Fluorescence microscopy has become an essential tool to study biological molecules, pathways and events in living cells, tissues and animals. Compared with other imaging techniques, such as electron microscopy, the main advantage of fluorescence microscopy is its compatibility with living cells, which allows dynamic and minimally invasive imaging experiments. The main weakness of fluorescence microscopy, however, has been its spatial resolution, which was limited to ~200 nm for many years.

At one end of the resolution spectrum, positron-emission tomography, magnetic resonance imaging and optical coherence tomography provide real-time read-out from animal or human subjects, but they cannot discern details smaller than ~1 mm, ~100 μm and ~10 μm, respectively (FIG. 1). At the opposite end, electron microscopy provides near molecular-level spatial resolution, but cells must be fixed, which is invasive and prevents dynamic imaging. Between these two resolution extremes, fluorescence microscopy provides a range of spatial and temporal resolutions. The most widely used fluorescence imaging methods, confocal microscopy and wide-field microscopy, can resolve certain cellular organelles (for example, the nucleus, the endoplasmic reticulum and the Golgi apparatus) and can track proteins and other biomolecules in live cells. The spatial resolution limit, however, prevents the resolution of single synaptic vesicles or pairs of interacting proteins. Many fields of biology would benefit from improved combinations of spatial and temporal resolution. For example, neuronal synaptic vesicles are ~40 nm in size and signalling occurs on the milliseconds timescale. Bacteria are only 1–5 μm in size, and subcellular features are difficult to resolve by conventional fluorescence microscopy.

We focus on the recent emergence of new far-field fluorescence imaging techniques, which theoretically have no limit to their spatial resolution. We describe the current limitations in terms of spatial and temporal resolution, and discuss how some of these might be overcome through improvements in fluorescent probe technology. In general, two classes of probes are used for super-resolution imaging: fluorescent proteins (FPs) and non-genetically encoded probes, such as organic small-molecule fluorophores and quantum dots. We describe the desired characteristics, strengths and weaknesses of each probe class. We also suggest future improvements to probe design and targeting, which might help to bring us closer to molecular-resolution imaging in live cells in real time.

Overcoming the diffraction limit

In 1873, Abbe observed that focused light always results in a blurred or diffracted spot, and the size of the spot places a fundamental limit on the minimal distance at which we can resolve two or more features[1] (TIMELINE). This spot is commonly represented by the point spread function (PSF). The mathematical expression for Abbe's finding is that the resolution of a fluorescence microscope is limited to $\lambda/2n\sin\alpha$ in the focal plane (xy) and $2\lambda/n\sin^2\alpha$ along the optical axis (z), where λ is the wavelength of the light used and $n\sin\alpha$ is the numerical

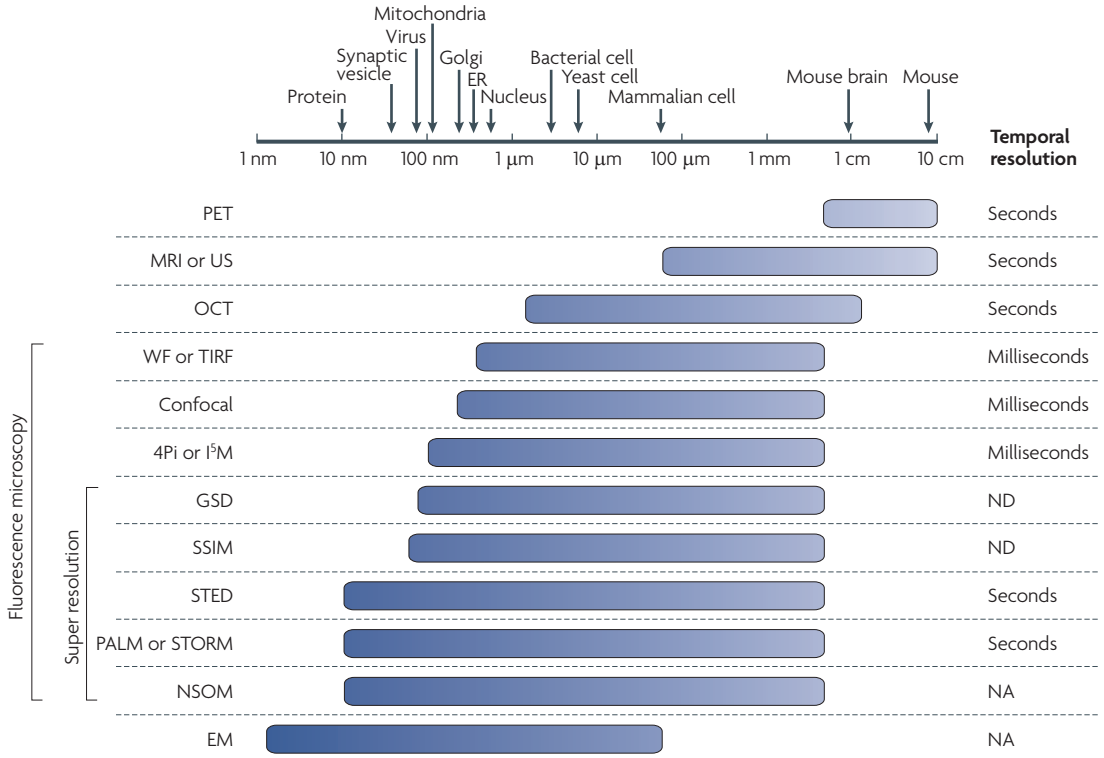

Figure 1 | **Comparison of the spatial and temporal resolutions of biological imaging techniques.** The size scale is logarithmic. Average sizes of biological features are given; specific sizes vary widely among different species and cell lines. The spatial and temporal resolutions are estimates of current practices, and some were taken from REF. 120. The spatial resolution is given for the focal plane. The temporal resolution is not applicable (NA) for electron microscopy (EM) or near-field scanning optical microscopy (NSOM) because they image static samples. Ground-state depletion (GSD) and saturated structured-illumination microscopy (SSIM) have not been shown on biological samples, and thus their temporal resolutions are not determined (ND). ER, endoplasmic reticulum; MRI, magnetic resonance imaging; OCT, optical coherence tomography; PALM, photoactivated localization microscopy; PET, positron-emission microscopy; STED, stimulated emission depletion; STORM, stochastic optical reconstruction microscopy; TIRF, total internal reflection fluorescence; US, ultrasound; WF, wide-field microscopy.

Positron-emission tomography
An *in vivo* imaging technique that detects the location of positron-emitting isotopes by the pair of γ-rays that are emitted when the positrons encounter electrons. The most common scan is produced by imaging the metabolic activity of fluorodeoxyglucose, a radioactive analogue of glucose.

Magnetic resonance imaging
A medical imaging technique in which the magnetic nuclei (especially protons) of a subject are aligned in a strong, uniform magnetic field, absorb energy from tuned radio frequency pulses and emit radio frequency signals as their excitation decays.

Optical coherence tomography
An *in vivo* imaging technique that sends out femtosecond infrared pulses and uses optical interference to sense reflections from tissue inhomogeneities.

Confocal microscopy
A mode of optical microscopy in which a focused laser beam is scanned laterally along the *x* and *y* axes of a specimen in a raster pattern. Point-like illumination and point-like detection results in a focal spot that is narrower than that obtained in wide-field microscopy.

Wide-field microscopy
The most popular mode of light microscopy, in which the entire specimen is bathed in light from a mercury or xenon source, and the image can be viewed directly by eye or projected onto a camera.

aperture of the lens. As most lenses have a numerical aperture of <1.5 (α is <70°), the theoretical resolution limit for cell imaging (where λ must be longer than ~400 nm to minimize harm to cells) is 150 nm laterally and 500 nm axially[2]. In fact, this is the current resolution obtainable with a wide-field microscope.

Because the axial resolution in wide-field microscopy is much poorer than the lateral resolution, research in microscopy instrumentation from the 1970s to the 1990s focused on the improvement of axial resolution (TIMELINE). Initially, the use of confocal[3] and multiphoton microscopy[4] provided optical sectioning but did not significantly improve axial resolution. Later, I^{5}M (REFS 5,6) and 4Pi (REFS 7–9) microscopies combined the apertures of two opposing lenses to allow the visualization of cellular structures with a large improvement in axial resolution — down to ~100 nm — using wide-field and confocal set-ups, respectively. Although axial resolution improved by sixfold, lateral resolution remained unchanged. It was not until the 1990s that fundamentally new microscopies revolutionized the imaging field, for the first time breaking the lateral resolution diffraction limit. These techniques are collectively named super-resolution imaging techniques.

Near-field super-resolution imaging. In 1992, a super-resolution image of a biological sample was obtained for the first time[10] (TIMELINE). Near-field scanning optical microscopy (NSOM) was originally proposed in 1928 by Synge[11], and was first demonstrated in 1984 using visible radiation on test slides[12,13]. NSOM overcomes the diffraction limit by removing the lenses and thus eliminates the need for focusing. Instead, the light passes through a small aperture that is positioned close to the sample (in the near-field zone), such that light cannot substantially diffract. The lateral resolution, determined by the diameter of the aperture, is typically 20–120 nm. Although NSOM has been used to study the nanoscale organization of several membrane proteins[14,15], imaging in the near-field is technically challenging. The aperture probe is difficult to make, and the need for feedback to maintain a constant distance from an irregular sample limits the speed of image acquisition. In addition, NSOM cannot be used for intracellular imaging. These factors have prevented widespread use of NSOM in cell biology.

Far-field super-resolution imaging. In contrast to NSOM, lenses are used in far-field microscopy, and they are placed at a distance from the sample. For super-resolution

imaging, the key to overcoming the diffraction limit is to spatially and/or temporally modulate the transition between two molecular states of a fluorophore (for example, a dark and a bright state). Some techniques achieve super resolution by narrowing the PSF of an ensemble image of many fluorophores. These techniques include stimulated emission depletion (STED)[16], ground-state depletion (GSD)[17], and saturated structured-illumination microscopy (SSIM)[18,19] and its recent combination with I^5M (I^5S) (REF. 20). Other super-resolution imaging techniques detect single molecules and rely on the principle that a single emitter can be localized with high accuracy if sufficient numbers of photons are collected[21]. These techniques include photoactivated localization microscopy (PALM)[22], fluorescence photoactivation localization microscopy (FPALM)[23] and stochastic optical reconstruction microscopy (STORM)[24] (TIMELINE).

Cell biology imaged at super resolution

We focus our attention on STED, PALM, FPALM and STORM techniques because of recent reports that show the ability of these techniques to achieve super resolution in biological samples (for an in-depth review of other high- and super-resolution imaging techniques see REF. 25). Several other techniques[26–29] have recently been developed but it is too early to assess their potential for biology.

Imaging an ensemble of molecules. STED was the first far-field super-resolution imaging technique to be applied to cell imaging[30]. To break the diffraction limit, STED uses spatially modulated and saturable transitions between two molecular states. Specifically, the sample is illuminated by two laser beams: an excitation laser pulse is immediately followed by a red-shifted pulse called the STED beam (FIG. 2Aa). Excited fluorophores exposed to the STED beam are almost instantly transferred back to their ground states by means of stimulated emission. This nonlinear (nearly exponential) de-excitation of the fluorescent state by the STED beam is the basis of breaking the diffraction limit in STED imaging. Although both laser pulses are diffraction-limited, the STED pulse is modified to feature a zero-intensity point at the focal centre and strong intensities at the spot periphery (creating, for example, a doughnut shape). If the two pulses are superimposed, only molecules that are close to the zero of the STED beam are allowed to fluoresce, thus confining the emission towards the zero. This effectively narrows the PSF (for example, to 65 nm in FIG. 2Aa), and ultimately increases resolution beyond the diffraction limit. To obtain a complete subdiffraction image, the central zero is scanned across the sample. Using this scheme, STED microscopy has achieved 20 nm resolution in the focal plane[31,32] and, recently, 45 nm resolution in all three dimensions[33].

Since its invention in 1994, STED has been applied to several cell biological problems. STED resolved synaptotagmin-I in individual synaptic vesicles (~40 nm in size), and showed that this protein forms isolated clusters upon vesicle fusion[34]. STED also revealed the ring-like structure of the protein bruchpilot at synaptic active zones in the *Drosophila melanogaster* neuromuscular junction[35], and the size and density of syntaxin-I clusters in PC12 cells[36]. Additionally, STED has enabled the visualization of the nuclear protein splicing component-35 (SC35)[31], the nicotinic acetylcholine receptor[37], the transient receptor potential channel M5 (TRPM5)[38] and the flotillin-2-induced clusters of the amyloid precursor protein[39]. Recently, STED was extended to two-colour imaging, enabling colocalization studies of two mitochondrial proteins[32]. This study required nanoscale-resolution imaging because the entire mitochondrion is only ~200–500 nm.

Impressively, Westphal and colleagues reported video-rate imaging of synaptic vesicles with 62 nm lateral resolution (FIG. 2Ab) in live hippocampal neurons[40]. Using STED microscopy, the synaptic vesicles, labelled with ATTO647N-conjugated anti-synaptotagmin antibodies, were observed to be highly restricted inside synaptic boutons. By contrast, vesicles outside boutons exhibit faster, linear movement, which might represent transit through axons (FIG. 2Ab). Time-lapse imaging of live mammalian cells with <50 nm lateral resolution was also recently achieved using the yellow FP citrine targeted to the endoplasmic reticulum[41]. In this report, the use of a FP instead of an antibody label enabled live-cell imaging of intracellular features.

Although many applications of STED have been reported, the instrumentation required is still complicated and this is the main limitation to its widespread use. This limitation has been acknowledged and STED microscopy using continuous wave beams was recently reported[42]. This has the potential to be implemented in any conventional confocal set-up. In addition, the use of a commercially available super-continuum laser system eliminates the need for two laser sources[43].

Imaging single molecules. PALM, FPALM and STORM are fundamentally different from STED in that they image single molecules. The basic principle behind these techniques is that the position of a single molecule can be localized to 1 nm accuracy or better if enough photons are collected and there are no other similarly emitting molecules within ~200 nm. This notion, which was described by Heisenberg in the 1930s and mathematically formulated in the 1980s[44], has enabled single-particle tracking studies, such as the imaging of the movement of kinesin-coated beads with a precision of 1–2 nm by Gelles *et al.*[45], and is the basis of many other single-molecule imaging studies.

Localization accuracy does not, however, directly translate into super-resolution images, especially for densely labelled samples; the overlapping images of these fluorophores would prevent their accurate localization. To overcome this, super-resolution imaging techniques determine the nanoscale localization of individual fluorescent molecules by sequentially switching them on and off using light of different wavelengths (FIG. 2Ba). In contrast to STED, in which the switching is predefined in space through the superimposition of the two laser beams, the switching is done stochastically

Point spread function
(PSF). A measure of the performance of an optical system. The PSF defines the apparent shape of a point target as it appears in the output image. For a fluorophore, PSF is a Gaussian function, whose full-width at half maximum (FWHM) defines the spatial resolution of the imaging system.

Multiphoton microscopy
A form of laser-scanning microscopy that uses the simultaneous absorption of two or more photons of a long wavelength to excite fluorophores that are normally excited by a single photon of shorter wavelength. This is a nonlinear imaging technique that enables deep penetration into thick tissues and reduces light damage.

Optical sectioning
The imaging of thin sections of a sample without the need to mechanically slice it. This is achieved by eliminating the excitation and/or detection of fluorescence that originates in the out-of-focus planes. Effectively, the distance between the closest and furthest objects in focus is greatly reduced to yield a clean optical section.

Ground state depletion
A mode of RESOLFT microscopy (see RESOLFT) that exploits the saturation of fluorophore transition from the ground state to the dark triplet state. A laser beam with a light intensity distribution featuring one or more zeros switches some of the fluorophores to their triplet state T_1 or another metastable dark state, while recording those that are still left or have returned to the ground state S_0.

Saturated structured-illumination microscopy
A mode of RESOLFT microscopy (see RESOLFT) that exploits the saturation of fluorophore transition from the ground state S_0 to the excited singlet state S_1. This differs from STED in that ultrasharp dark regions of molecules are created with steeply surrounded regions of molecules in the bright state.

Timeline | **Development of super-resolution imaging techniques and applications to cell biology**

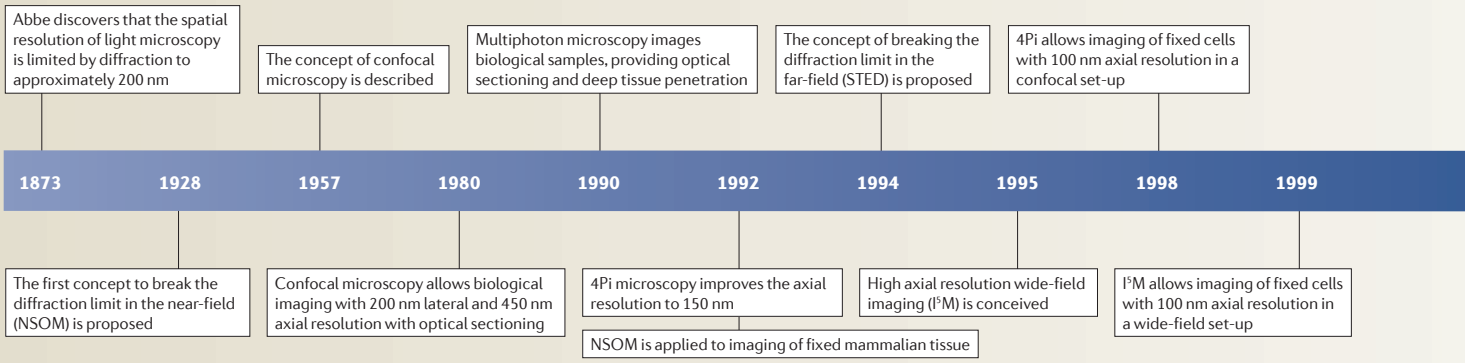

FPALM, fluorescence photoactivation localization microscopy; NSOM, near-field scanning optical microscopy; PALM, photoactivated localization microscopy; PALMIRA, PALM with independently running acquisition; STED, stimulated emission depletion; STORM, stochastic optical reconstruction microscopy.

in single-molecule-based super-resolution methods. In each imaging cycle, most molecules remain dark, but a small percentage of molecules are stochastically switched on, imaged and then localized. Repeating this process for many cycles allows the reconstruction of a super-resolution image.

Such super-resolution techniques have been used to image protein–DNA complexes *in vitro*[24] and to image molecular structures, such as lysosomes, mitochondria and adhesion complexes[22], and microtubules and clathrin coated pits[46] in fixed cells. Single-molecule-based super-resolution microscopy has also been extended to multicolour imaging[46–48]. Two-colour STORM revealed the organization of microtubule networks and clathrin-coated pits in fixed mammalian cells with ~20 nm resolution[46] (FIG. 2Bb). Using PALM (FIG. 2Ca), two-colour imaging of actin and adhesion complexes in fixed cells was reported[48] (see FIG. 2Cb, which shows fibrillar-like adhesions of paxillin running parallel to actin fibres). At nanoscale resolution, little overlap is observed between actin and paxillin, although actin bundles densely cluster around some but not all paxillin adhesions (FIG. 2Cb). This structural relationship could not be viewed using conventional microscopy.

Three-dimensional (3D) super-resolution imaging has also been achieved with STORM and FPALM. Using optical astigmatism, Huang and co-workers performed STORM imaging with 20–30 nm resolution in the *xy* plane and 50 nm resolution in the axial dimension[49]. Using multifocal plane imaging, Juette and co-workers achieved 3D FPALM imaging with 30 nm resolution in the *xy* plane and 75 nm resolution in the axial dimension[50].

Recently, PALM and FPALM have been extended to live-cell imaging[51–53]. For example, Hess and colleagues imaged the distribution of the membrane protein haemagglutinin from influenza virus in live fibroblasts with ~40 nm accuracy, and determined an effective diffusion coefficient of 0.1 μm per second[51]. Manley *et al.* imaged individual tsO45 vesicular stomatitis virus G particles and HIV-1 Gag membrane proteins in living cells, and obtained high-density molecular tracks[52]. Shroff and colleagues imaged adhesion-complex dynamics in live CHO cells with 60 nm resolution at an imaging speed of 25–60 seconds per frame[53]. They observed the migration of adhesion complexes away from the cell edge, which had previously been seen by conventional microscopy. However, super resolution allowed them to observe, for the first time, that the rear end of migrating adhesion complexes moves faster than the front. Also, new adhesion complexes form in the cell interior rather than at the cell edge.

Limitations of super-resolution imaging

Super-resolution microscopy has improved both lateral and axial resolutions, recently achieving ~50–70 nm resolution in all three dimensions[33,49,50]. However, we are far from molecular resolution (1–5 nm), in which individual molecules in a macromolecular assembly can be resolved. What factors determine the spatial resolution limit for each of these methods?

Ensemble super-resolution imaging. In STED, the resolution depends on the extent of the saturation of emission depletion, because this defines the degree to which the PSF can be narrowed (FIG. 2Aa). This relationship is given by equation 1:

$$\text{Spatial resolution} = \Delta x = \frac{\lambda}{2n\sin\alpha \times \left(1 + \frac{I^{max}}{I^{sat}}\right)^{1/2}} \quad (1)$$

In this equation, λ is the wavelength, $n\sin\alpha$ is the numerical aperture of the microscope, I^{max} is the applied intensity of the STED pulse and I^{sat} is the STED intensity that gives 50% depletion of the emission[31]. It therefore follows that to maximize the saturation of emission depletion (I^{max}/I^{sat}) and improve STED resolution, one needs to either increase the intensity of the STED pulse (increase I^{max}) or decrease the intensity needed to send a particular fluorophore to the dark state (decrease I^{sat}). For example, a typical I^{max} intensity used in early STED studies of ~250 MW per cm^2 produced a lateral resolution of

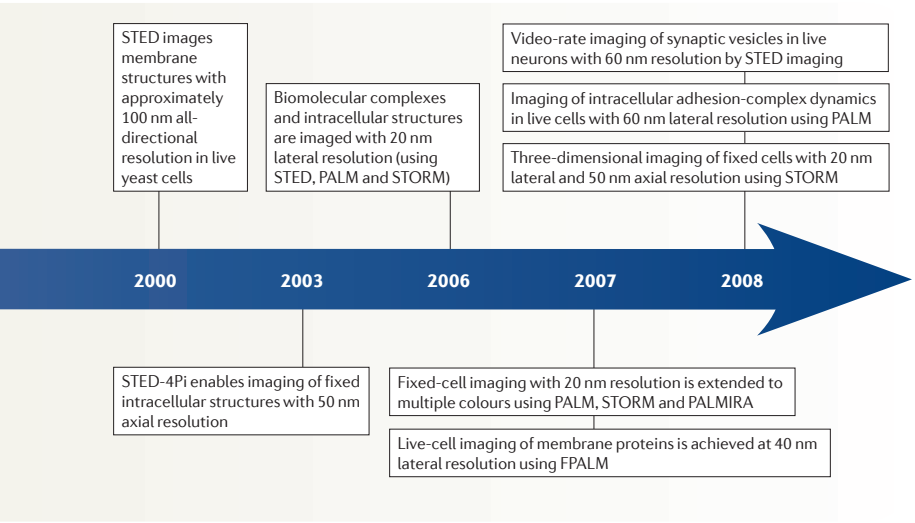

50–70 nm for the fluorescent small molecule ATTO532 (REF. 31). Increasing I^{max} above this value was not possible because the probe photobleached too quickly. Later, the use of STED pulses of longer duration (to reduce ground-state multiphoton absorption)[54] and of lower frequency (to allow the triplet state to relax and avoid triplet-state excitation)[31] resulted in a marked decrease in fluorophore photobleaching. These improvements enabled the increase of I^{max} to ~2,200 MW per cm^2 and resulted in 15–20 nm resolution for the same dye[31].

Because there will always be an upper limit to I^{max} that is imposed by probe photobleaching and sample damage, an alternative approach is to decrease I^{sat} (a separate characteristic of each fluorophore). I^{sat} defines the intensity at which the rate of stimulated depletion is faster than other competing interstate transitions, such as fluorescence emission or excitation to higher (singlet or triplet) excited states, and I^{sat} is inversely proportional to both the fluorescence lifetime of the fluorophore and its cross-section for emission depletion. Thus, good STED dyes are characterized by high quantum yields, emission spectra that match the STED wavelength, enhanced photostability, long fluorescence lifetimes (>0.8 ns)[55] and a low cross-section for multiphoton absorption and for absorption by the excited states.

Another approach to decrease I^{sat} is to change the nature of the 'bright' and 'dark' states of the probe. We described above a stimulated depletion that brings the molecule from the excited state S_1 (bright) to the ground state S_0 (dark), but STED can also work if, for example, the two states are two different molecular states of a photoswitchable probe. This more general approach to super-resolution imaging is termed reversible saturable optically linear fluorescence transitions (RESOLFT)[56], which applies to all ensemble techniques based on a stimulated transition between any two molecular states (for example, STED, SSIM and GSD). Because the spontaneous interstate transition is almost non-existent when using photoswitchers, I^{sat} is much smaller and therefore the resolution can be improved, even with low laser intensities. This was first shown by Hofmann *et al.*[56], who obtained 50–100 nm resolution in the focal plane using the photoswitchable protein FP595 (isolated from *Anemonia sulcata*; BOX 1) with a STED power of only 100–600 W per cm^2, which is six orders of magnitude lower than that used for ATTO532 (REF. 31), and similar to the intensities used, for example, in FPALM imaging[51].

It is also advantageous to maximize the speed of super-resolution imaging, to allow the study of dynamic processes in living cells. Initial acquisition times for PALM, FPALM, STED and STORM super-resolution techniques were of the order of minutes to hours, which restricted them to the imaging of fixed samples. Recently, STED was applied to imaging of synaptic vesicle movements in living cells at video rate, or 28 frames per second[40]. The imaging speed in STED is restricted by the minimum number of photons that can be collected per pixel and per unit time. The high imaging speed in STED was obtained at the cost of increasing laser intensity (to 400 MW per cm^2) and reducing the number of photons collected per imaging cycle, which caused a reduction in spatial resolution (to 62 nm) as well as field of view (to 2.5 μm × 1.8 μm). The goal is to achieve this same video-rate imaging speed while maximizing spatial resolution and using laser intensities that are more appropriate for living cells.

Single-molecule-based super-resolution imaging. In PALM, FPALM and STORM, spatial resolution is determined by the number of photons that can be collected from each fluorophore and by the background fluorescence, as given by equation 2:

$$\Delta x = \frac{k_1}{N^{1/2}} + \frac{k_2 b}{N} \qquad (2)$$

In this equation, Δx is the localization precision; k_1 and k_2 are determined by the excitation wavelength, the numerical aperture of the objective and pixel size; N is the number of collected photons (a fraction of the total emitted photons); and b is the background noise per pixel[21]. Thus, to maximize resolution, the aim is to minimize background noise and maximize photon output of the fluorophore. For example, in the absence of background, if 10,000 photons can be collected from a single fluorophore molecule before it bleaches or is turned off, its localization can be determined to ~2 nm precision, and 400 photons can provide 10–20 nm localization accuracy[57]. Background can arise from sample autofluorescence, as well as from residual fluorescence of surrounding probe molecules in the dark state. For single-molecule-based super-resolution imaging, it is then desirable for fluorophores to have a high contrast ratio, which is defined as the emission intensity ratio between the bright versus dark states. This is because at low contrast ratios, the collective fluorescence from dark molecules can obscure the signal from the small number of bright molecules during each imaging cycle. One way to reduce background is by using a total internal reflection fluorescence (TIRF) microscope, but this restricts imaging to the cell membrane. To maximize spatial resolution, it is also important to maximize the signal from fluorophores in the bright state. Thus, brighter fluorophores with high extinction coefficients and high quantum yields are desirable.

Reversible saturable optically linear fluorescence transitions
(RESOLFT). A mode of light microscopy that exploits the saturation of a reversible single photon transition from a dark state to a bright state, or vice versa. A light intensity distribution featuring zeros creates arbitrarily sharp regions of molecules in the dark or the bright states; the bright regions allow the assembly of a subdiffraction image. The spatial resolution is no longer limited by the wavelength of the light in use, but rather is determined by the saturation that can be realized.

Photoswitcher
A molecule that can reversibly switch between two molecular states on irradiation with light of a specific wavelength and intensity. Currently known fluorescent photoswitchers are photoactivatable molecules that switch between a dark and a fluorescent state upon illumination.

Total internal reflection fluorescence
A microscopy technique that is designed to probe the surface of fluorescently labelled living cells with an evanescent wave. This wave is generated by a light beam that strikes between two media of differing refractive indices at an angle beyond the critical angle.

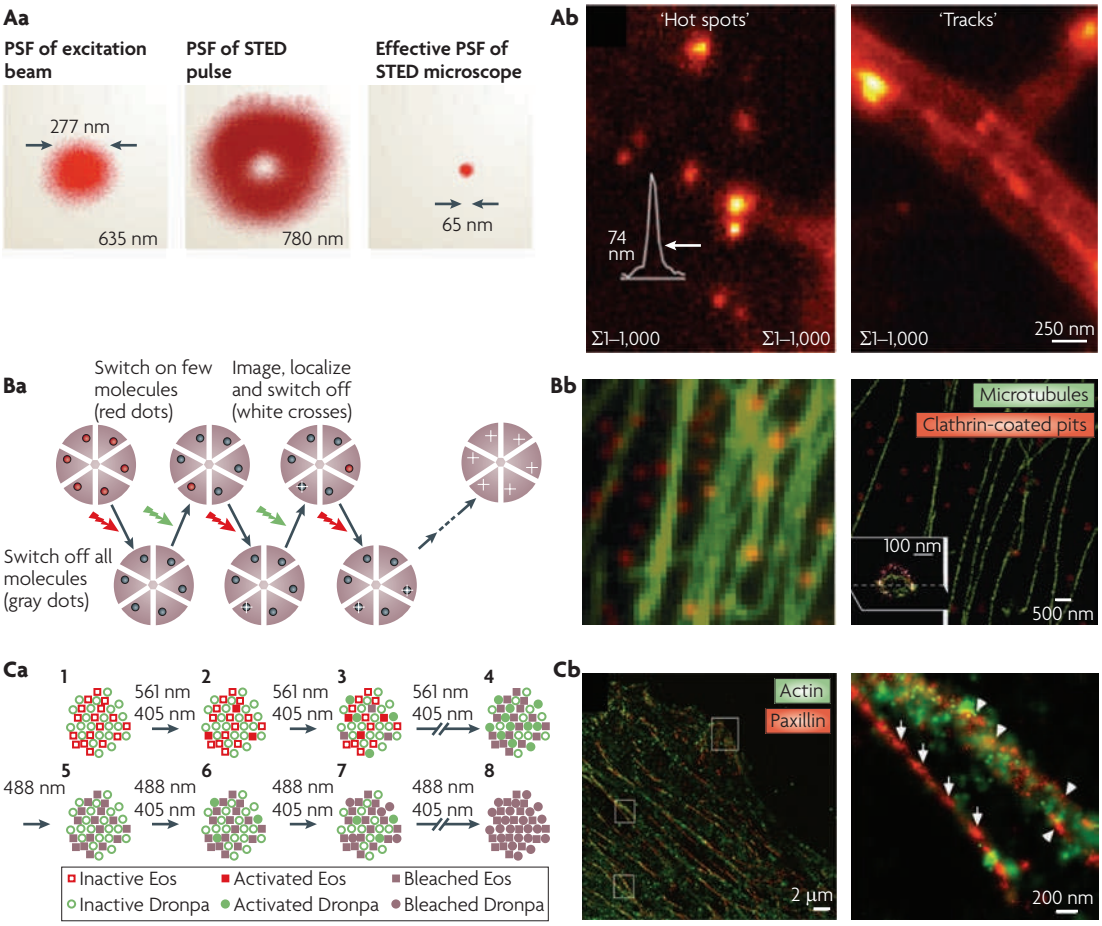

Figure 2 | **Cellular features imaged by super-resolution techniques. Aa** | Point spread function (PSF) of stimulated emission depletion (STED) microscopy. The focal spot of excitation light (bright red) is overlapped with a doughnut-shaped red-shifted light (dark red), which quenches excited molecules in the excitation spot periphery. This confines emission to a central spot. Scanning this central spot (called the zero) across the sample results in a subdiffraction image. **Ab** | Synaptic vesicle movement imaged with STED. Synaptic vesicles were immunolabelled in live neurons, and the movement of each vesicle was individually recorded; the sum of 1,000 individual movie frames (Σ1–1,000) depicts the movement of various synaptic vesicles. **Ba** | Stochastic optical reconstruction microscopy (STORM). The fluorescence image is constructed from highly precise localization of single molecules. In each imaging cycle, all fluorescent molecules in the field of view are switched off by, for example, a strong red laser. Only a small percentage of them are then switched on (green light) such that their images do not overlap, and their emission is recorded (red light) and used to localize their positions (white crosses) with nanometre accuracy. **Bb** | Multicolour and three-dimensional (3D) STORM imaging. Conventional (left panel) and STORM (right panel) images of immunostained microtubules (green) and clathrin-coated pits (red) in the same region of a BSC-1 cell. A 3D STORM image of a clathrin-coated pit is inset. An *xy* cross-section and an *xz* cross-section of the pit are shown in perspective. **Ca** | Photoactivated localization microscopy (PALM). PALM follows the same principle as STORM. To perform two-colour PALM imaging, the orange emitters (Eos fluorescent protein) are sequentially activated (405 nm light), imaged (561 nm light), localized and bleached until a subdiffraction image can be constructed (steps 1–3). After bleaching the remaining Eos molecules (step 4), the many active green emitters (Dronpa fluorescent protein) are first deactivated with a strong 488-nm light (step 5). Then, the green emitters are activated, imaged and bleached (steps 6–8). **Cb** | Two-colour PALM images show the nanostructural organization of cytoskeletal actin (green) and the adhesion protein paxillin (red) in an HFF-1 cell. Actin bundles densely cluster around some (arrowheads) but not all (full arrows) paxillin adhesions. Images in part **Aa** modified, with permission, from REF. 32 © (2007) The Biophysical Society. Images in part **Ab** modified, with permission, from REF. 40 © (2008) American Association for the Advancement of Science. Part **Ba** modified, with permission, from *Nature Methods* REF. 24 © (2006) Macmillan Publishers Ltd. All rights reserved. Images in part **Bb** modified, with permission, from REF. 46 © (2007) American Association for the Advancement of Science. Inset image in part **Bb** modified, with permission, from REF. 49 © (2008) American Association for the Advancement of Science. Parts **Ca**,**Cb** modified, with permission, from REF. 48 © (2007) National Academy of Sciences.

This need for low background and high photon output highlights some of the main differences between single-molecule and ensemble read-out schemes. A main advantage of the single-molecule-based super-resolution strategy is that the marker molecules are not forced to undergo several photoswitching cycles — this is the case for ensemble-based super-resolution imaging, in which photobleaching is a major problem. However, the

Box 1 | **Fluorescent proteins used for super-resolution imaging**

Fluorescent proteins (FPs) that are used for super-resolution imaging can be divided into three classes: irreversible photoactivatable FPs (PA-FPs), whose fluorescence can be turned on with light of a specific wavelength; photoshiftable FPs (PS-FPs), whose fluorescence excitation and emission spectra shift following illumination; and reversible PA-FPs (also known as photoswitching FPs), whose emission can be reversibly switched on and off with light. For example, exposure to ultraviolet (UV) or blue light causes an irreversible spectral shift in the PS-FP Eos[110] from a green state to an orange state (see figure, part **a**). As another example, the reversible PA-FP Dronpa[111] fluoresces green in its bright state (see figure, part **b**). Prolonged or intense irradiation with green light leads to a non-fluorescent form with absorption maximum at 390 nm, which can then be reversibly photoactivated back to the green-emitting form by irradiation with 405 nm light. Dronpa can undergo 100 cycles of activation–quenching with only a 25% loss of its original fluorescence[59].

The photophysical properties of PA-FPs and PS-FPs used for super-resolution imaging vary widely (see table). Activating light refers to the irradiation used for the photoactivation or photoshifting event; quenching light reverts the FP to its dark state (this is only applicable to reversible proteins); pre/post colours refer to the colours before and after photoshifting (or photoactivation). The following photophysical properties all correspond to the fluorescent form of the FPs after activation or shifting: λ_{ex}, excitation wavelength; λ_{em}, emission wavelength; ε_{abs}, extinction coefficient; η_{fl}, fluorescence quantum yield; contrast, fold increase in fluorescence at λ_{em} after photactivation or photoshifting; *N*, number of detected photons per single molecule of FP in each activation or shifting imaging cycle; NA, not applicable; ND, not determined.

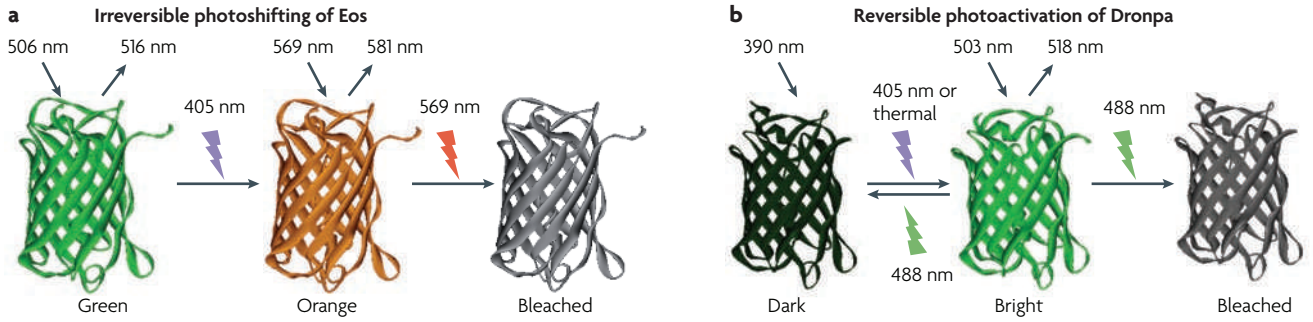

Fluorescent protein	Activating light	Quenching light	Pre/post colours	λ_{ex} (nm)	λ_{em} (nm)	ε_{abs} ($M^{-1}cm^{-1}$)	η_{fl} (%)	Contrast	*N*	Oligomeric state	Refs
Irreversible photoactivatable fluorescent proteins											
PA-GFP	UV-violet	NA	Dark/green	504	517	17,400	79	200	ND	Monomer	51,61,62
PA-RFP1-1	UV-violet	NA	Dark/red	578	605	10,000	8	ND	ND	Monomer	60,61,64
Photoshiftable fluorescent proteins											
PS-CFP2	UV-violet	NA	Cyan/green	490	511	47,000	23	>2,000	260	Monomer	48,61,69, 112
Kaede	UV-violet	NA	Green/orange	572	582	60,400	33	2,000	~400	Tetramer	22,61,65
KiKGR	UV-violet	NA	Green/red	583	593	32,600	65	>2,000	ND	Tetramer	61,66
Monomeric Eos	UV-violet	NA	Green/orange	569	581	37,000	62	ND	~490	Monomer	22,48,52, 53,61,68
Dendra-2	Blue	NA	Green/orange	553	573	35,000	55	4,500	ND	Monomer	68,112
Reversible photoactivatable fluorescent proteins											
FP595	Green	450 nm	Dark/red	590	600	59,000	7	30	ND	Tetramer	56,70
Dronpa	UV-violet	488 nm	Dark/green	503	518	95,000	85	ND	120	Monomer	48,59,61
Padron	Blue	405 nm	Dark/green	503	522	43,000	64	ND	ND	Monomer	71

fluorescent 'on' state must produce enough photons to allow its precise localization (which is predetermined in STED imaging). In addition, the single-molecule approach requires strict control over the maximum density of photoactivated molecules, and depends on their reliable localization against a diffuse background.

Spatial resolution should be improved without sacrificing temporal resolution. Live-cell PALM was recently used to study adhesion-complex dynamics[53], but this was made possible by the slow intrinsic motion of adhesion complexes. At an imaging rate of 25–60 seconds per frame, many other biological movements would appear to be blurred. To improve the temporal resolution of PALM, FPALM and STORM, it is necessary to maximize the number of photons that can be collected per unit area per unit time. Manley *et al.*[52] reported that high-density single-particle tracking with PALM was best achieved using EosFP, which has the largest contrast ratio and highest photon output of all the known photoshiftable FPs[22,48].

Another consideration is that when using irreversible fluorophores, temporal resolution is also limited by the photobleaching rate. In these cases, less photostable probes are desired, although a balance must be met

between faster photobleaching and adequate photons to achieve high localization accuracy. In other words, irreversible probes should be very bright but not necessarily photostable. The alternative is to use reversible fluorophores such as cyanine (Cy) dyes[58] or the PA-FP Dronpa[59], which can be turned off and thus do not have to be photobleached.

FPs for super-resolution imaging

Although simple FPs, such as green FP (GFP) and yellow FP (YFP), have been used in STED imaging[41,55], most super-resolution imaging techniques exploit the intrinsic ability of certain FPs to change their spectral properties on irradiation with light of a specific wavelength. There are two main classes of FPs used in super-resolution imaging: those that convert from a dark state to a bright fluorescent state (PA-FPs), and those that change fluorescence wavelength on irradiation (photoshiftable FPs (PS-FPs)) (reviewed in REFS 60,61) (BOX 1). All known PS-FPs irreversibly shift their wavelength but PA-FPs can photoactivate either reversibly or irreversibly.

Desired characteristics. FPs for super-resolution imaging should be as bright as possible (that is, have large extinction coefficients (ε_{abs}) and large fluorescence quantum yields (η_{fl})), to maximize the number of detectable photons per molecule (N) and they should have high contrast ratios. Additionally, the spontaneous interconversion rates into and out of the activated (fluorescent) state must be low compared with the light-controlled activation rate. The rates of photobleaching (for irreversible PS-FPs) or deactivation (for reversible switchers) should be balanced with the activation rate to ensure that, only a small number of molecules are in the fluorescent state at any given time, so that on average they are separated by more than the diffraction limit, and also to ensure that each activated molecule remains in the fluorescent state for long enough to give sufficient photons for accurate localization. Finally, for cellular studies, the FP should be monomeric to minimize perturbation of the target protein. As seen below, every currently available modulatable FP has at least one drawback.

Irreversible PA-FPs. Two irreversible PA-FPs have been engineered: PA-GFP and monomeric PA-RFP1-1. PA-GFP was the first to be engineered, developed by mutagenesis of the original GFP[62]. Although PA-GFP has been used in FPALM imaging to determine the diffusion coefficient of haemagglutinin in live fibroblasts[51], its green fluorescence and low contrast ratio results in high background, which limits spatial resolution to ~40 nm and necessitates a minimum acquisition time of ~150 ms per frame (about sevenfold slower than the acquisition time required for rsFastLime (also known as Dronpa V157G), a variant of the reversible PA-FP Dronpa[63]). The low contrast ratio and extremely low quantum yield of the only irreversible red PA-FP, monomeric PA-RFP1-1 (REF. 64) (BOX 1), which is derived from DsRed, have thus far prevented its use in super-resolution imaging.

Irreversible PS-FPs. Many of the naturally occurring and engineered PS-FPs exhibit a shift from green to red emission (BOX 1). Among these, the natural PS-FP kaede[65] and the engineered KikGR[66] are obligate tetramers, and are thus not suitable for imaging of cellular proteins. EosFP is the most commonly used red PS-FP for super-resolution imaging, as it has the highest contrast and brightness and has been engineered into a monomeric form that is suitable for protein fusion (Eos; BOX 1)[67]. EosFP was used in one of the first demonstrations of PALM imaging[22], and it was later used in combination with PS-CFP2 and Dronpa in two-colour PALM imaging experiments[48]. It was because of the optimal photophysical properties of EosFP that Manley and co-workers could perform single-particle tracking of membrane proteins in live COS7 cells at an imaging speed of 20 frames per second[52]. EosFP in its original dimeric form was also used in the latest demonstration of PALM in live cells[53]. The main disadvantage of monomeric Eos, however, is that chromophore formation occurs only at temperatures below 30°C, which limits its use in mammalian cells[67]. In this regard, Dendra-2, with similar contrast and brightness, could potentially outperform monomeric Eos, because it matures properly at 37°C and can be activated by blue light (which causes less damage to tissue than the ultraviolet (UV) light that is required for monomeric Eos)[68]. However, even the brightest PS-FP is still much dimmer than some small-molecule organic fluorophores. For example, Eos provides ~490 collected photons per molecule[48], whereas the switchable fluorophore pair Cy3–Cy5 provides ~6,000 collected photons per molecule per switching cycle and lasts ~200 switching cycles[46,58].

The only green-emitting PS-FP, PS-CFP2 (REF. 69), is preferred in multicolour studies because it has the highest contrast ratio and yields the largest number of photons of all of the green modulatable FPs[48] (BOX 1).

Reversible PA-FPs. Reversible PA-FPs (also known as photoswitchers) are advantageous in super-resolution imaging because the same fluorophore can be imaged multiple times. Reversible photoswitching is mandatory in RESOLFT imaging, in which each molecule is switched on and off many times in order to reconstruct a subdiffraction image.

The first reversible PA-FP reported was FP595 (REF. 70). Although FP595 has low contrast and is tetrameric, it was successfully used by Hofmann *et al.* to achieve 50–100 nm focal plane resolution using RESOLFT imaging[56]. The best-known reversible PA-FP is the naturally occurring Dronpa[59] and its many engineered variants. Unfortunately, although Dronpa exhibits a large extinction coefficient and quantum yield, its fluorescence is excited with 488 nm light, which also inactivates the protein, therefore resulting in a low number of collected photons per imaging cycle. Higher spatial resolution can be obtained with PS-CFP2 than with Dronpa[48].

To overcome this limitation, Andresen and co-workers recently engineered a Dronpa variant with positive-switching characteristics[71]. In contrast to Dronpa, this

Extinction coefficient
The (molar) extinction coefficient (ε_{abs})of a species is defined by the equation $A = \varepsilon bc$, where A is the absorbance of the solution, b is the path length and c is the concentration of the species. The fluorescence brightness of a species is proportional to the product of its molar extinction coefficient and fluorescence quantum yield.

Fluorescence quantum yield
The ratio of photons emitted to photons absorbed. The fluorescence brightness of a species is proportional to the product of its molar extinction coefficient and fluorescence quantum yield.

new variant, called Padron, is activated and imaged by blue light, whereas UV light switches the protein off. It remains to be seen how the protein behaves for super-resolution imaging. As an additional example of how probe development combined with instrumentation advances can lead to improvements in imaging, Egner and co-workers have recently shown that the use of a faster photoswitching variant of the FP Dronpa, rsFastLime[72], in combination with asynchronous recording, accelerates imaging acquisition and eliminates the need for TIRF in PALM. The intense light used in this setting drives most of the fluorophores into a dark state. Individual fluorophores then stochastically and spontaneously revert to the bright state, briefly emit a burst of photons, then revert to the dark state. In this scheme, the acquisition time matches the mean duration of an emission burst, producing rapid acquisition and lower background fluorescence. This procedure has been termed PALMIRA (PALM with independently running acquisition)[47,63,73].

Finally, the recent engineering of the first monomeric red reversible PA-FP, rsCherry, has opened new possibilities for multicolour time-lapse imaging. Live-cell PALMIRA imaging of the endoplasmic reticulum labelled with rsCherry provided images with ~75 nm lateral resolution[74]. As described for Padron, the authors have also engineered a positive-switching version of monomeric cherry, termed rsCherryRev, which might further enhance its use, although its applicability to cell imaging has not been shown[74].

In summary, FPs can be targeted with absolute specificity but they are generally bigger, dimmer and less photostable than small-molecule fluorophores. This low brightness usually makes it necessary to use a TIRF microscope to minimize background fluorescence. Even with the brightest PS-FP, EosFP, the maximum frame rate that can be achieved (~25 seconds per frame) is still too slow to image most biological processes if a resolution of ~60 nm is desired. Brighter FPs are needed to increase temporal resolution without losing spatial resolution. Unfortunately, although the mechanisms of photoswitching for some FPs have been recently described[61], the strict requirement for chromophore formation inside the β-barrel of FPs makes the engineering of brighter FPs a difficult task and highlights the need for the discovery of new FPs from other species. Additionally, new monomeric proteins of different colours are needed to allow routine multicolour imaging at super resolution.

Non-genetically encoded probes

Three main classes of non-genetically encoded probes have been used in super-resolution imaging: inorganic quantum dots (BOX 2), reversible photoactivatable fluorophores (also known as photoswitchers) and irreversible photoactivatable fluorophores (also known as photocaged fluorophores) (BOX 3). STED imaging initially used regular small-molecule dyes, in which the probe was imaged in its excited state and the surrounding molecules were quenched by the STED pulse that sent them to ground state. In this type of imaging scheme, the intensity of the STED pulse needs to be extremely high to compete with the spontaneous fluorescence decay of the probe — molecules with both high quantum yield and long fluorescence lifetime (slow fluorescence decay), such as the ATTO or DY dyes, are ideal[30–32,34–38,40,42] (BOX 3). Later, STED imaging evolved into the more general RESOLFT imaging, which uses photoswitchers, such as FP595 (REF. 56), and furyl fulgides[75].

Reversible PA probes. The small-molecule analogues to reversible PA-FPs (such as Dronpa and rsCherry[74]) are photochromic probes, including rhodamines and diarylethenes, as well as photoswitchable cyanines. The switching mechanism of a photochromic rhodamine B (PC-RHB) is depicted in BOX 3. Irradiation of the closed isomer with UV light or with red light (for pulsed two-photon absorption) results in transient formation of a coloured and brightly fluorescent open isomer[73]. The reaction is thermally reverted by heat within milliseconds to minutes, depending on the solvent. Irradiation of the fluorescent isomer with green light excites fluorescence emission but does not regenerate the non-fluorescent state. This property makes the photochromic rhodamine superior to Dronpa (similar to Padron and rsCherryRev), because the fluorescence signal can be read without the undesired erasing side effect, which results in higher photon output per switching event. Photochromic rhodamines also provide an example of how probe development can lead to improvements in the imaging process. Folling and co-workers[76] reported the design of a new probe based on rhodamine 590 (PC-RH590), whose extra rigidity improves cross-section compared to the original PC-RHB[73] for two-photon absorption. Efficient two-photon activation could also be achieved with this probe, and fluorescent images with 15 nm resolution in the focal plane were obtained[76].

Other photochromic molecules, such as photochromic diarylethenes[77], could potentially be used in super-resolution imaging, but they have limited water solubility, which restricts their biological utility.

Photoswitchable cyanine dyes have been used in both PALMIRA[47] and STORM[24,46,49] imaging. Although it has also been used alone[47], Cy5 is best used in combination with a secondary chromophore that facilitates the switching[46,58]. For example, when Cy5 is paired with Cy3, the same red laser that excites Cy5 is also used to switch the dye to a stable dark state. Subsequent exposure to green laser light converts Cy5 back to the fluorescent state, and this recovery rate depends on the close proximity of the secondary dye Cy3 (called the activator)[58]. Cy5 switching can also be facilitated by other activator fluorophores, such as Alexa Fluor 405 and Cy2 (REF. 46). Furthermore, Cy3 was found to facilitate switching of other cyanines, such as Cy5.5 and Cy7 (REF. 46). This finding greatly increases the palette of colours that are available for STORM imaging and has allowed simultaneous visualization of microtubules and clathrin-coated pits in fixed mammalian cells with 20–30 nm lateral resolution[46] (FIG. 2Bb). This availability of several colours contrasts with the lack thereof for modulatable FPs. Unfortunately, the development

Box 2 | **Quantum dots as probes for super-resolution imaging**

Quantum dots (QDs) are a class of non-genetically encoded probes that are commonly used in single-molecule imaging owing to their enhanced photostability and extreme brightness. QDs are inorganic semiconductor nanocrystals, typically composed of a cadmium selenide (CdSe) core and a zinc sulphide (ZnS) shell and whose excitons (excited electron-hole pairs) are confined in all three dimensions, which gives rise to characteristic fluorescent properties. For biological applications, QDs are coated with a passivating layer to improve solubility, and are conjugated to targeting biomolecules, such as antibodies or streptavidin (see figure, part **a**). As fluorescent probes, QDs are characterized by broad absorption profiles, high extinction coefficients and narrow and spectrally tunable emission profiles. Small CdSe QD cores (2.3 nm diameter) emit blue light, whereas larger crystals (5.5 nm diameter) emit red light, producing size-dependent optical properties[114] (see figure, part **b**).

Irvine and co-workers recently reported the ability to switch on and off a certain kind of QD, thus rendering this type of QD suitable for super-resolution imaging[115]. They showed that the fluorescence of manganese (Mn)-doped ZnSe QDs can be reversibly depleted with ~90% efficiency using a continuous-wave modulation laser of ~2 MW per cm^2. The main novelty of this report is that modulation is achieved directly by light and relies only on internal electronic transitions, without the need for an external photochromic activator or quencher. Thus, this type of QD can be used in super-resolution imaging in the same way as small-molecule organic photoswitchers (see the main text). The figure in part **c** shows a comparison between the images obtained using RESOLFT (reversible saturable optically linear fluorescence transitions) (top left panel) or conventional confocal microscopy (top right panel). The fluorescence intensity profile through a representative RESOLFT point spread function (yellow dashed line) shows that *in vitro* imaging of the QDs using RESOLFT resulted in ~45 nm lateral resolution, a vast improvement over the corresponding confocal image (lower panel). I_{fluo}, fluorescence intensity; *y*, direction or axis. Part **a** modified, with permission, from *Nature Methods* REF. 113 © (2008) Macmillan Publishers Ltd. All rights reserved. Image (by F. Frankel) in part **b** reproduced, with permission, from REF. 114 © (2007) Chemical Society. Part c, reproduced, with permission, from REF. 115 © (2008) Wiley-VCH.

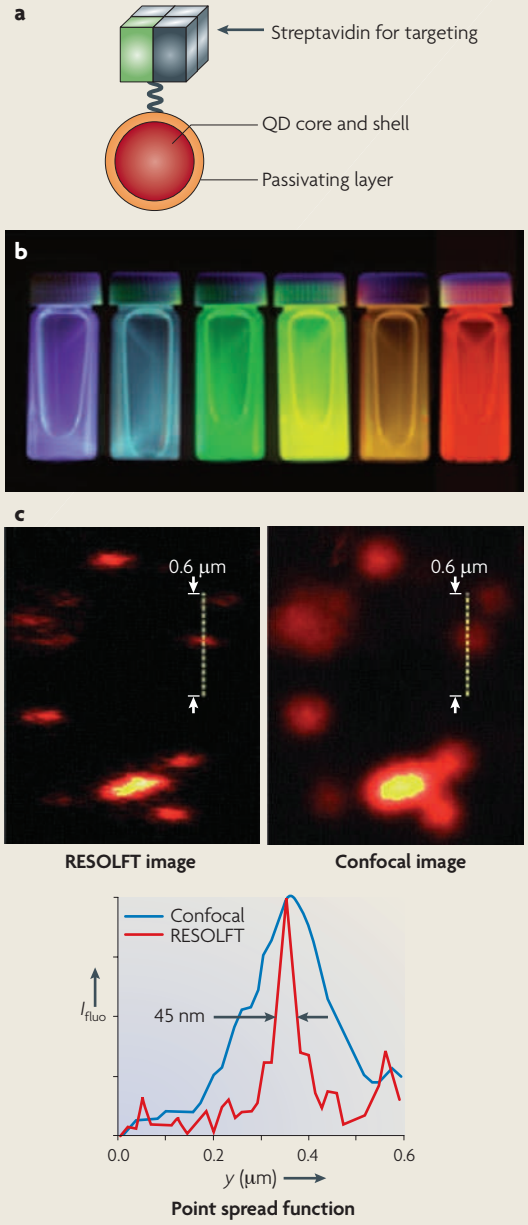

of improved switching pairs is currently hindered by the fact that the switching mechanism of these dyes is unknown. Finally, the recently developed Cy3–Cy5 double conjugate facilitates labelling[78].

When compared with their FP counterparts (FP595, Dronpa and Padron; BOX 1), photoswitchable dyes have larger contrast ratios, and they have higher extinction coefficients, which results in brighter probes with higher numbers of collected photons per molecule. Of the photoswitchable probes, rhodamines stand out because of their potential for intracellular labelling in live cells, as they are membrane permeable (sulphonated cyanine dyes are not). Improvements are required, however, to reduce the known affinity of rhodamines for intracellular organelles that is caused by their hydrophobicity and positive charge.

Irreversible PA probes. Caged compounds, such as caged Q-rhodamine[79,80], can also be exploited in super-resolution imaging (BOX 3). During uncaging, irradiation with UV light causes the release of a protective group and results in a large increase in the fluorescence intensity of the dye. Photocaged probes can be used in PALM, FPALM or STORM in the same way as irreversible PA-FPs: they can be uncaged, localized with high precision and then bleached. Caging can be a way of generating new PA probes that are based on fluorophores with otherwise good photophysical properties but without intrinsic photoswitching ability. The potential of caged compounds was first shown by Betzig and co-workers, who used PALM to image caged rhodamine–dextran that had been dried on glass cover slips[22]. Caged fluorescein

Box 3 | **Small-molecule fluorophores for super-resolution imaging**

Three classes of small-molecule fluorophores have been used for super-resolution imaging: regular non-shifting, non-activatable fluorescent dyes; reversible photoactivatable molecules (also called photoswitchers); and irreversible photoactivatable compounds (also called photocaged fluorophores). Unlike photoshiftable fluorescent proteins, there have been no reports to date of organic compounds that are capable of photoshifting between two different wavelengths. Among regular fluorescent probes, ATTO dyes (see figure, top left panel) have been widely used in stimulated emission depletion (STED) imaging owing to their intense brightness, high photostability and long fluorescence lifetimes. However, reversible saturable optically linear fluorescence transitions (RESOLFT), photoactivated localization microscopy (PALM), fluorescence photoactivation localization microscopy, PALM with independently running acquisition (PALMIRA) and stochastic optical reconstruction microscopy (STORM) rely on modulatable fluorophores, and thus make use of reversible and irreversible photoactivatable probes. Within the photoswitchers class, the photoactivation of cyanine (Cy) dyes can be facilitated by a second chromophore molecule (called the activator). Photochromic molecules, such as rhodamine B (see figure, top right panel) can photoswitch independently, without the addition of other molecules, via light-induced isomerization[73]. Among photocaged organic fluorophores, caged Q-rhodamines (see figure, bottom panel) and caged fluorescein have been used for super-resolution imaging[22,50]. It must be noted that reversible photoswitchers are advantageous for single-molecule super-resolution imaging because the same fluorophore can be used multiple times. Indeed, reversible photoswitching is mandatory in RESOLFT imaging.

A comparison can be made between the photophysical properties of selected small-molecule fluorophores used in super-resolution imaging (see table). Colour refers to the colour of emitted light in the fluorescent 'on' state; ε_{abs} extinction coefficient; η_{fl}, fluorescence quantum yield; λ_{ex}, excitation maximum wavelength; λ_{em}, emission maximum wavelength; τ_{fl}, fluorescence lifetime; IR, infrared; *N*, number of detected photons per single molecule in each imaging cycle; ND, not determined; UV, ultraviolet.

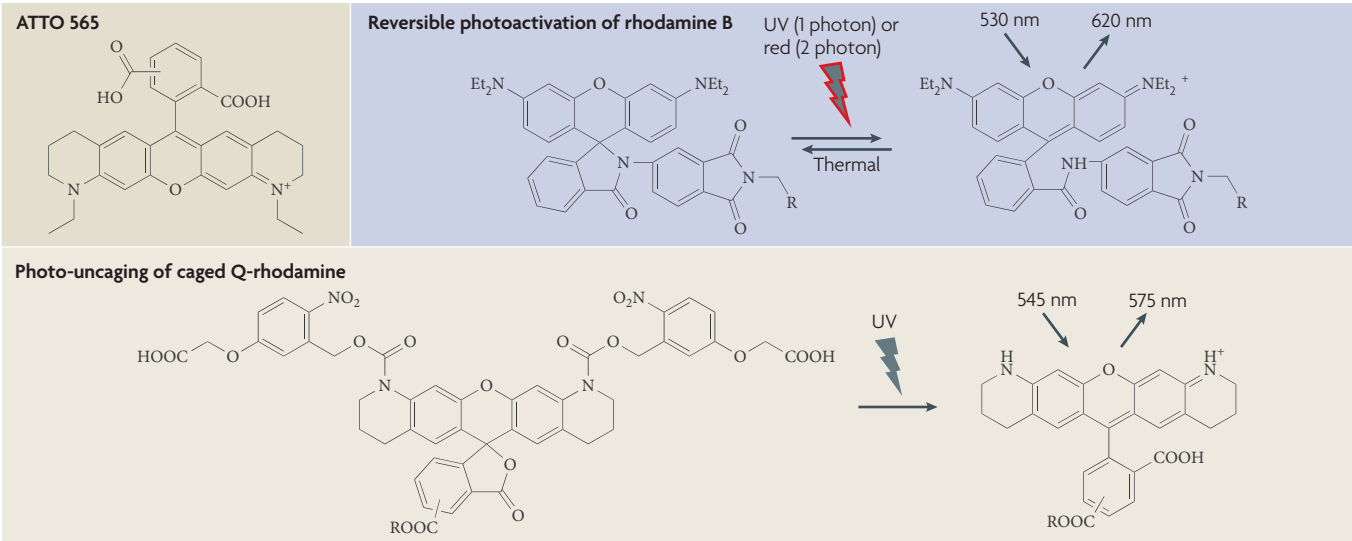

	Colour	λ_{ex} (nm)	λ_{em} (nm)	ε_{abs} ($M^{-1}cm^{-1}$)	η_{fl} (%)	τ_{fl} (ns)	*N*	Used for	Refs
Regular fluorescent dyes									
ATTO532	Orange	532	553	115,000	90	3.8	ND	STED	31,32§
Photoswitchers									
Rhodamine B	Red	530	620	105,000	65	ND	750	PALMIRA	73
Alexa Fluor 647*	Red	650	665	240,000	33	1.0	6,000	STORM	46‖
Cy5*	Red	649	664	250,000	28	1.0	6,000	STORM	46¶
Cy5.5*	Red	675	694	190,000	23	1.0	6,000	STORM	46¶
Cy7*	Near IR	747	767	200,000	28	<0.3	~1,000	STORM	46¶
Photocaged fluorophores									
Caged Q-rhodamine	Red	545	575	90,000	90	ND	ND	PALM	22,79,80‖
Caged carboxyfluorescein	Green	494	518	29,000‡	93	4.6	ND	FPALM	50,80,116‖

*Photoactivation of these fluorophores is strongly facilitated by the presence of an activator fluorophore, such as Cy2, Cy3 or Alexa Fluor 405, to induce photoswitching.‡The extinction coefficient is estimated at physiological pH. §Information also from Atto-tec. ‖Information also from Invitrogen. ¶Information also from GE healthcare.

has also been used to image beads, achieving sub-100 nm resolution in all directions[50]. A new irreversible photoactivatable compound based on a dicyanodihydrofuran fluorophore has been developed by Lord *et al.*[81], who reported photoactivation and live-cell imaging of the dye in mammalian cells, although not with super resolution. Caged compounds have not yet been used for super-resolution imaging of biological samples.

Box 4 | **Methods for site-specific targeting of small-molecule probes to cellular proteins**

Small-molecule fluorophores can be advantageous over their fluorescent protein counterparts owing to their enhanced brightness and photostability. However, they are not genetically encodable, which complicates their targeting. Several methods have been developed for targeting of organic fluorophores to specific proteins in live cells (see table). One approach (see figure, left panel) is to fuse the target protein to a peptide or protein recognition sequence, which then recruits the small molecule. In general, protein recognition domains offer greater targeting specificity but larger bulk than peptide recognition domains[117,118]. Another approach (see figure, right panel) is enzyme-mediated protein labelling. A recognition peptide is fused to the protein of interest and a natural or engineered enzyme ligates the small-molecule probe to the recognition peptide. This approach can give highly specific and rapid labelling, with the benefit of a small directing peptide sequence.

AGT, O^6-alkylguanine-DNA alkyltransferase; AP, biotin ligase acceptor peptide; Cy, cyanine dye; DHFR, dihydrofolate reductase; FKBP12, 12 kDa FK506-binding protein; LAP, lipoic acid ligase acceptor peptide; NA, not applicable; NTA, nitrilotriacetic acid; OG, oregon green; PPTases, phosphopantetheine transferases; QD, quantum dot; SNARF1, seminaphthorhodafluor-1; TMR, tetramethylrhodamine.

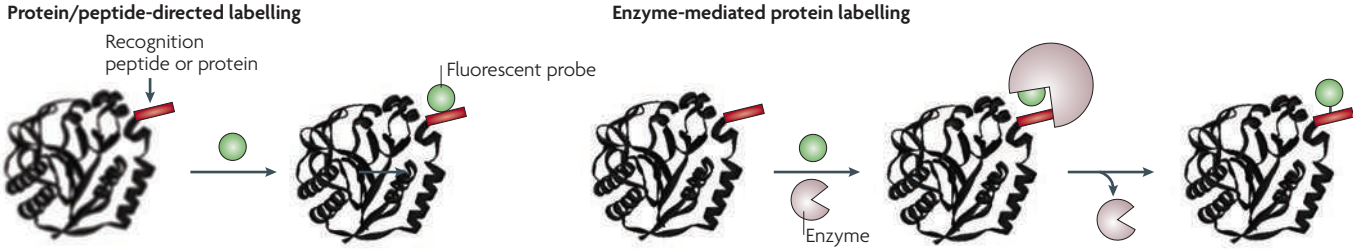

Recognition sequence	Enzyme used	Size of recognition sequence (aa)	Covalent attachment	Fluorophores demonstrated	Cellular proteins labelled	Refs
Protein or peptide-directed labelling methods						
TetraCys	NA	6–10	Yes	Fluorescein (FlAsH), resorufin (ReAsH) and CHoAsH	Membrane* and intracellular	82,83, 118,119
HexaHis	NA	6–12	No	NTA-I and II, OG488, Cy7 and ATTO647 or 565	Membrane	84–86
PolyAsp	NA	8–16	No‡	Fluorescein, TMR and Cy5	Membrane	87–89
Bungarotoxin-binding peptide	NA	13	No	Rhodamine	Membrane	90,91
FKBP12 (F36V)	NA	98	No	Fluorescein	Membrane	92
DHFR	DHFR	157	No	Fluorescein, bodipy and TexasRed	Intracellular	93,94
SNAP-tag and CLIP-Tag	AGT	182	Yes	Fluorescein, TMR Cy and SNARF1	Membrane and intracellular	95–97
Cutinase	Cutinase	200	Yes	AlexaFluor and QDs	Membrane	98
HaloTag	Dehalogenase	296	Yes	Fluorescein, TMR, AlexaFluor and OG488	Membrane and intracellular	99
Enzyme-mediated labelling methods						
SorTag	Sortase A	6	Yes	AlexaFluor and TMR	Membrane	100,101
Q-tag	Transglutaminase	7	Yes	Fluorescein	Membrane	102
A1/S6	AcpS or Sfp PPTases	11	Yes	AlexaFluor, Cy and TexasRed	Membrane	106
AP	Biotin ligase	15	Yes	Fluorescein, AlexaFluor and QD	Membrane	103–105
LAP	Lipoic acid ligase	12–17	Yes	AlexaFluor, Cy3, coumarin, fluorescein	Membrane and intracellular	107,108

*Cell-surface protein labelling using the tetraCys tag requires reducing agents. ‡A covalent version of the polyAsp tag has recently been developed[88].

Targeting methods for non-genetically encoded probes. Although non-genetically encoded probes generally show increased brightness and photostability compared with FPs, they also have disadvantages. The lack of genetic encoding means that these probes require a means to target them to the biomolecule of interest inside cells. These probes have been traditionally targeted using antibody conjugation, although this has many disadvantages. Antibodies are not membrane permeable, and hence are not useful for intracellular labelling of living cells. Antibody staining also usually results in low labelling efficiency and the large size of antibodies adds uncertainty (~10–20 nm) to the spatial relationship between the label and its target. Why does labelling efficiency matter? The label–target relationship was recently described by Shroff and co-workers by

Nyquist criterion
The sampling frequency should be equal or larger than twice the largest frequency that is to be recorded.

analogy with the Nyquist criterion; the distance between two labelled molecules must be smaller than half of the desired spatial resolution[53]. If we want a spatial resolution of 5 nm, we need to have labelled molecules at least every 2 nm. Given the bulk and weak affinity of many antibodies, it is difficult to achieve such labelling density. Another disadvantage of many non-genetically encoded probes is their inability to permeate through the cell membrane, which restricts their use to either fixed cells or cell-surface proteins.

In order to fully realize the intrinsic imaging resolution of super-resolution techniques, we need to develop strategies to target small molecules without significantly increasing the size of the tag and with high labelling efficiency. BOX 4 describes some of the current approaches for site-specific protein labelling in live cells. In a subset of these methods, the protein of interest is fused to a peptide or protein sequence that recruits the small molecule. Examples of methods that use a peptide tag include the tetraCys[82,83,118], hexaHis[84–86], the polyAsp[87–89] and the bungarotoxin-binding peptide[90,91] methodologies. Some other methodologies use proteins to recruit the small-molecule probe, such as the FKBP12 protein[92] and the enzymes dihydrofolate reductase (DHFR)[93,94], O^6-alkylguanine-DNA alkyltransferase (AGT)[95–97], cutinase[98] and dehalogenase[99]. The use of protein tags, instead of peptide tags, can improve the specificity of the binding owing to the larger interaction surface area that they can establish with the recruited probe, but the cost is the increased size of the tag, which can perturb protein function.

To bridge the requirements of high labelling specificity and minimal perturbation of the target protein, a second set of methodologies uses a peptide recognition sequence but then uses an enzyme to catalyse the covalent attachment of the probe to the peptide (BOX 4). Using an enzyme to catalyse probe ligation improves the specificity of the labelling and also gives faster and covalent attachment of the probe. Examples of this second approach include the methods based on the enzymes sortase[100,101], transglutaminase[102], biotin ligase[103–105], phosphopantetheine transferases (Sfp and AcpS)[106] and lipoic acid ligase[107,108].

Conclusions and future perspectives

These are exciting times in cell biology because live-cell imaging with molecular resolution (1–5 nm) is now closer to becoming a reality. The recent development of super-resolution imaging techniques has enabled the visualization of cellular features with previously unimagined detail. STED imaging has allowed real-time tracking of single synaptic vesicles in cultured hippocampal neurons[40] and has revealed the anatomy and dynamics of syntaxin-I clusters in PC12 cells[36]. STED, STORM, PALM and FPALM allowed cellular structures to be imaged in 3D and in multiple colours[32,33,46-50,109]. At such an improved resolution, colocalization of protein pairs has been reported that contradicts previous reports based on low-resolution imaging[48], and diffusion properties of membrane proteins have been mapped to high resolution[51,52].

We have described the technological advances introduced by the STED, PALM, FPALM and STORM techniques, which have made far-field super-resolution imaging possible. We have also pointed out the future developments that we think are required to further improve the spatial and temporal resolution of these methods. Although improved computational methods and imaging equipment are also needed, fluorescent probes do limit performance of super-resolution imaging. In the future, we expect that smaller, brighter, more photostable and membrane-permeable fluorescent probes will allow video-rate imaging with molecular resolution.

1. Abbe, E. Beitrage zur Theorie des Mikroskops und der mikroskopischen Wahrmehmung. *Arc. F. Mikr. Anat.* **9**, 413–420 (1873) (in German).
2. Hell, S. W., Dyba, M. & Jakobs, S. Concepts for nanoscale resolution in fluorescence microscopy. *Curr. Opin. Neurobiol.* **14**, 599–609 (2004).
3. Cavanagh, H. D., Petroll, W. M. & Jester, J. V. The application of confocal microscopy to the study of living systems. *Neurosci. Biobehav. Rev.* **17**, 483–498 (1993).
4. Denk, W., Strickler, J. H. & Webb, W. W. Two-photon laser scanning fluorescence microscopy. *Science* **248**, 73–76 (1990).
5. Gustafsson, M. G. L., Agard, D. A. & Sedat, J. W. Sevenfold improvement of axial resolution in 3D wide-field microscopy using two objective lenses. *Proc. Soc. Photo Opt. Instrum. Eng.* **2412**, 147–156 (1995).
6. Gustafsson, M. G. L., Agard, D. A. & Sedat, J. W. I^5M: 3D widefield light microscopy with better than 100nm axial resolution. *J. Microsc.* **195**, 10–16 (1999).
7. Bahlmann, K., Jakobs, S. & Hell, S. W. 4Pi-confocal microscopy of live cells. *Ultramicroscopy* **87**, 155–164 (2001).
8. Hell, S. W. & Stelzer, E. H. K. Fundamental improvement of resolution with a 4Pi-confocal fluorescence microscope using two-photon excitation. *Opt. Comm.* **93**, 277–282 (1992).
9. Schrader, M., Bahlmann, K., Giese, G. & Hell, S. W. 4Pi-confocal imaging in fixed biological specimens. *Biophys. J.* **75**, 1659–1668 (1998).
10. Betzig, E. & Trautman, J. K. Near-field optics: microscopy, spectroscopy, and surface modification beyond the diffraction limit. *Science* **257**, 189–195 (1992).
11. Synge, E. H. A suggested method for extending the microscopic resolution into the ultramicroscopic region. *Phil. Mag.* **6**, 356–362 (1928).
12. Lewis, A., Isaacson, M., Harootunian, A. & Murray, A. Development of a 500 Å spatial resolution light microscope. *Ultramicroscopy* **13**, 227–231 (1984).
13. Pohl, D. W., Denk, W. & Lanz, M. Optical stethoscopy: image recording with resolution λ/20. *Appl. Phys. Lett.* **44**, 651–653 (1984).
14. de Lange, F. *et al.* Cell biology beyond the diffraction limit: near-field scanning optical microscopy. *J. Cell Sci.* **114**, 4153–4160 (2001).
15. de Bakker, B. I. *et al.* Nanometer-scale organization of the α subunits of the receptors for IL2 and IL15 in human T lymphoma cells. *J. Cell Sci.* **121**, 627–633 (2008).
16. Hell, S. W. & Wichmann, J. Breaking the diffraction resolution limit by stimulated emission: stimulated-emission-depletion fluorescence microscopy. *Opt. Lett.* **19**, 780–782 (1994).
17. Hell, S. W. & Kroug, M. Ground-state-depletion fluorescence microscopy — a concept for breaking the diffraction resolution limit. *Appl. Phys. B* **60**, 495–497 (1995).
18. Gustafsson, M. G. Nonlinear structured-illumination microscopy: wide-field fluorescence imaging with theoretically unlimited resolution. *Proc. Natl Acad. Sci. USA* **102**, 13081–13086 (2005).
19. Heintzmann, R., Jovin, T. M. & Cremer, C. Saturated patterned excitation microscopy—a concept for optical resolution improvement. *J. Opt. Soc. Am. A Opt. Image Sci. Vis.* **19**, 1599–1609 (2002).
20. Shao, L. *et al.* I^5S: widefield light microscopy with 100-nm-scale resolution in three dimensions. *Biophys. J.* **94**, 4971–4983 (2008).
21. Thompson, R. E., Larson, D. R. & Webb, W. W. Precise nanometer localization analysis for individual fluorescent probes. *Biophys. J.* **82**, 2775–2783 (2002).
22. Betzig, E. *et al.* Imaging intracellular fluorescent proteins at nanometer resolution. *Science* **313**, 1642–1645 (2006).
Together with references 24 and 31, biological imaging with a lateral resolution of ~20 nm was achieved for the first time. First demonstration of single-molecule-based super-resolution imaging in fixed cells.
23. Hess, S. T., Girirajan, T. P. & Mason, M. D. Ultra-high resolution imaging by fluorescence photoactivation localization microscopy. *Biophys. J.* **91**, 4258–4272 (2006).
24. Rust, M. J., Bates, M. & Zhuang, X. Sub-diffraction-limit imaging by stochastic optical reconstruction microscopy (STORM). *Nature Methods* **3**, 793–795 (2006).
Together with references 22 and 31, biological imaging with a lateral resolution of ~20 nm was achieved for the first time. First demonstration of single-molecule-based super-resolution imaging of biomolecules and molecular complexes.
25. Hell, S. W. Far-field optical nanoscopy. *Science* **316**, 1153–1158 (2007).

Review of the physical principles that underlie most high- and super-resolution imaging techniques.
26. Stark, P. R., Halleck, A. E. & Larson, D. N. Breaking the diffraction barrier outside of the optical near-field with bright, collimated light from nanometric apertures. *Proc. Natl Acad. Sci. USA* **104**, 18902–18906 (2007).
27. Chung, E., Kim, D., Cui, Y., Kim, Y. H. & So, P. T. Two-dimensional standing wave total internal reflection fluorescence microscopy: superresolution imaging of single molecular and biological specimens. *Biophys. J.* **93**, 1747–1757 (2007).
28. Lang, M. C., Engelhardt, J. & Hell, S. W. 4Pi microscopy with linear fluorescence excitation. *Opt. Lett.* **32**, 259–261 (2007).
29. Sharonov, A. & Hochstrasser, R. M. Wide-field subdiffraction imaging by accumulated binding of diffusing probes. *Proc. Natl Acad. Sci. USA* **103**, 18911–18916 (2006).
30. Klar, T. A., Jakobs, S., Dyba, M., Egner, A. & Hell, S. W. Fluorescence microscopy with diffraction resolution barrier broken by stimulated emission. *Proc. Natl Acad. Sci. USA* **97**, 8206–8210 (2000).
31. Donnert, G. *et al.* Macromolecular-scale resolution in biological fluorescence microscopy. *Proc. Natl Acad. Sci. USA* **103**, 11440–11445 (2006).
Together with references 22 and 24, biological imaging with a lateral resolution of ~20 nm was achieved for the first time. Understanding of fluorophore photophysics to reduce photobleaching enabled this breakthrough for STED imaging.
32. Donnert, G. *et al.* Two-color far-field fluorescence nanoscopy. *Biophys. J.* **92**, L67–L69 (2007).
33. Schmidt, R. *et al.* Spherical nanosized focal spot unravels the interior of cells. *Nature Methods* **5**, 539–544 (2008).
34. Willig, K. I., Rizzoli, S. O., Westphal, V., Jahn, R. & Hell, S. W. STED microscopy reveals that synaptotagmin remains clustered after synaptic vesicle exocytosis. *Nature* **440**, 935–939 (2006).
Excellent example of how super-resolution imaging can reveal previously unavailable details in neurobiology.
35. Kittel, R. J. *et al.* Bruchpilot promotes active zone assembly, Ca^{2+} channel clustering, and vesicle release. *Science* **312**, 1051–1054 (2006).
36. Sieber, J. J. *et al.* Anatomy and dynamics of a supramolecular membrane protein cluster. *Science* **317**, 1072–1076 (2007).
37. Kellner, R. R., Baier, C. J., Willig, K. I., Hell, S. W. & Barrantes, F. J. Nanoscale organization of nicotinic acetylcholine receptors revealed by stimulated emission depletion microscopy. *Neuroscience* **144**, 135–143 (2007).
38. Lin, W., Margolskee, R., Donnert, G., Hell, S. W. & Restrepo, D. Olfactory neurons expressing transient receptor potential channel M5 (TRPM5) are involved in sensing semiochemicals. *Proc. Natl Acad. Sci. USA* **104**, 2471–2476 (2007).
39. Schneider, A. *et al.* Flotillin-dependent clustering of the amyloid precursor protein regulates its endocytosis and amyloidogenic processing in neurons. *J. Neurosci.* **28**, 2874–2882 (2008).
40. Westphal, V. *et al.* Video-rate far-field optical nanoscopy dissects synaptic vesicle movement. *Science* **320**, 246–249 (2008).
Video-rate imaging of synaptic vesicles with 60 nm lateral resolution. Fastest super-resolution recording reported to date.
41. Hein, B., Willig, K. I. & Hell, S. W. Stimulated emission depletion (STED) nanoscopy of a fluorescent protein-labeled organelle inside a living cell. *Proc. Natl Acad. Sci. USA* **105**, 14271–14276 (2008).
42. Willig, K. I., Harke, B., Medda, R. & Hell, S. W. STED microscopy with continuous wave beams. *Nature Methods* **4**, 915–918 (2007).
43. Wildanger, D., Rittweger, E., Kastrup, L. & Hell, S. W. STED microscopy with a supercontinuum laser source. *Opt. Express* **16**, 9614–9621 (2008).
44. Bobroff, N. Position measurement with a resolution and noise-limited instrument. *Rev. Sci. Instrum.* **57**, 1152–1157 (1986).
45. Gelles, J., Schnapp, B. J. & Sheetz, M. P. Tracking kinesin-driven movements with nanometre-scale precision. *Nature* **331**, 450–453 (1988).
46. Bates, M., Huang, B., Dempsey, G. T. & Zhuang, X. Multicolor super-resolution imaging with photo-switchable fluorescent probes. *Science* **317**, 1749–1753 (2007).
Created nine distinguishable fluorescent probes based on photoswitchable cyanines, which enabled multicolour imaging of microtubules and clathrin-coated pits in fixed cells.
47. Bock, H. *et al.* Two-color far-field fluorescence nanoscopy based on photoswitchable emitters. *Appl. Phys. B* **88**, 161–165 (2007).
48. Shroff, H. *et al.* Dual-color superresolution imaging of genetically expressed probes within individual adhesion complexes. *Proc. Natl Acad. Sci. USA* **104**, 20308–20313 (2007).
Nanoscale resolution imaging of different adhesion complex proteins revealed little protein overlap, although they had been previously seen as colocalized using conventional microscopy. This work provides a rigorous analysis of the characteristics of several photoactivatable and photoshiftable FPs.
49. Huang, B., Wang, W., Bates, M. & Zhuang, X. Three-dimensional super-resolution imaging by stochastic optical reconstruction microscopy. *Science* **319**, 810–813 (2008).
STORM imaging combined with optical astigmatism enabled, for the first time, sub-100 nm resolution imaging in all three directions: ~25 nm lateral resolution and ~50 nm axial resolution.
50. Juette, M. F. *et al.* Three-dimensional sub-100 nm resolution fluorescence microscopy of thick samples. *Nature Methods* **5**, 527–529 (2008).
51. Hess, S. T. *et al.* Dynamic clustered distribution of hemagglutinin resolved at 40 nm in living cell membranes discriminates between raft theories. *Proc. Natl Acad. Sci. USA* **104**, 17370–17375 (2007).
First demonstration of super-resolution imaging in live cells. FPALM was used to track the movement of haemagglutinin molecules on the surface of a living cell with 40 nm accuracy.
52. Manley, S. *et al.* High-density mapping of single-molecule trajectories with photoactivated localization microscopy. *Nature Methods* **5**, 155–157 (2008).
53. Shroff, H., Galbraith, C. G., Galbraith, J. A. & Betzig, E. Live-cell photoactivated localization microscopy of nanoscale adhesion dynamics. *Nature Methods* **5**, 417–423 (2008).
Live-cell PALM super-resolution imaging is demonstrated on whole adhesion complexes using the photoshiftable EosFP.
54. Dyba, M. & Hell, S. W. Photostability of a fluorescent marker under pulsed excited-state depletion through stimulated emission. *Appl. Opt.* **42**, 5123–5129 (2003).
55. Willig, K. I. *et al.* Nanoscale resolution in GFP-based microscopy. *Nature Methods* **3**, 721–723 (2006).
56. Hofmann, M., Eggeling, C., Jakobs, S. & Hell, S. W. Breaking the diffraction barrier in fluorescence microscopy at low light intensities by using reversibly photoswitchable proteins. *Proc. Natl Acad. Sci. USA* **102**, 17565–17569 (2005).
57. Yildiz, A. *et al.* Myosin V walks hand-over-hand: single fluorophore imaging with 1.5-nm localization. *Science* **300**, 2061–2065 (2003).
58. Bates, M., Blosser, T. R. & Zhuang, X. Short-range spectroscopic ruler based on a single-molecule optical switch. *Phys. Rev. Lett.* **94**, 108101 (2005).
59. Ando, R., Mizuno, H. & Miyawaki, A. Regulated fast nucleocytoplasmic shuttling observed by reversible protein highlighting. *Science* **306**, 1370–1373 (2004).
60. Lippincott-Schwartz, J. & Patterson, G. H. Fluorescent proteins for photoactivation experiments. *Methods Cell Biol.* **85**, 45–61 (2008).
61. Lukyanov, K. A., Chudakov, D. M., Lukyanov, S. & Verkhusha, V. V. Innovation: photoactivatable fluorescent proteins. *Nature Rev. Mol. Cell Biol.* **6**, 885–891 (2005).
62. Patterson, G. H. & Lippincott-Schwartz, J. A photoactivatable GFP for selective photolabeling of proteins and cells. *Science* **297**, 1873–1877 (2002).
63. Egner, A. *et al.* Fluorescence nanoscopy in whole cells by asynchronous localization of photoswitching emitters. *Biophys. J.* **93**, 3285–3290 (2007).
64. Verkhusha, V. V. & Sorkin, A. Conversion of the monomeric red fluorescent protein into a photoactivatable probe. *Chem. Biol.* **12**, 279–285 (2005).
65. Ando, R., Hama, H., Yamamoto-Hino, M., Mizuno, H. & Miyawaki, A. An optical marker based on the UV-induced green-to-red photoconversion of a fluorescent protein. *Proc. Natl Acad. Sci. USA* **99**, 12651–12656 (2002).
66. Tsutsui, H., Karasawa, S., Shimizu, H., Nukina, N. & Miyawaki, A. Semi-rational engineering of a coral fluorescent protein into an efficient highlighter. *EMBO Rep.* **6**, 233–238 (2005).
67. Wiedenmann, J. *et al.* EosFP, a fluorescent marker protein with UV-inducible green-to-red fluorescence conversion. *Proc. Natl Acad. Sci. USA* **101**, 15905–15910 (2004).
68. Gurskaya, N. G. *et al.* Engineering of a monomeric green-to-red photoactivatable fluorescent protein induced by blue light. *Nature Biotech.* **24**, 461–465 (2006).
69. Chudakov, D. M. *et al.* Photoswitchable cyan fluorescent protein for protein tracking. *Nature Biotech.* **22**, 1435–1439 (2004).
70. Lukyanov, K. A. *et al.* Natural animal coloration can be determined by a nonfluorescent green fluorescent protein homolog. *J. Biol. Chem.* **275**, 25879–25882 (2000).
71. Andresen, M. *et al.* Photoswitchable fluorescent proteins enable monochromatic multilabel imaging and dual color fluorescence nanoscopy. *Nature Biotech.* **26**, 1035–1040 (2008).
Development of blue-shifted and positive-switching Dronpa variants enabled two-colour super-resolution imaging in *Escherichia coli* as well as monochromatic, multilabel imaging.
72. Stiel, A. C. *et al.* 1.8 Å bright-state structure of the reversibly switchable fluorescent protein Dronpa guides the generation of fast switching variants. *Biochem. J.* **402**, 35–42 (2007).
73. Folling, J. *et al.* Photochromic rhodamines provide nanoscopy with optical sectioning. *Angew. Chem. Int. Ed. Engl.* **46**, 6266–6270 (2007).
74. Stiel, A. C. *et al.* Generation of monomeric reversibly switchable red fluorescence proteins for far-field fluorescence nanoscopy. *Biophys. J.* **95**, 2989–2997 (2008).
75. Bossi, M., Folling, J., Dyba, M., Westphal, V. & Hell, S. W. Breaking the diffraction resolution barrier in far-field microscopy by molecular optical bistability. *New J. Phys.* **8**, 275–284 (2006).
76. Folling, J. *et al.* Fluorescence nanoscopy with optical sectioning by two-photon induced molecular switching using continuous-wave lasers. *Chemphyschem* **9**, 321–326 (2008).
77. Fukaminato, T. *et al.* Photochromism of diarylethene single molecules in polymer matrices. *J. Am. Chem. Soc.* **129**, 5932–5938 (2007).
78. Conley, N. R., Biteen, J. S. & Moerner, W. E. Cy3–Cy5 covalent heterodimers for single-molecule photoswitching. *J. Phys. Chem. B* **112**, 11878–11880 (2008).
79. Gee, K. R., Weinberg, E. S. & Kozlowski, D. J. Caged Q-rhodamine dextran: a new photoactivated fluorescent tracer. *Bioorg. Med. Chem. Lett.* **11**, 2181–2183 (2001).
80. Mitchison, T. J., Sawin, K. E., Theriot, J. A., Gee, K. & Mallavarapu, A. Caged fluorescent probes. *Methods Enzymol.* **291**, 63–78 (1998).
81. Lord, S. J. *et al.* A photoactivatable push-pull fluorophore for single-molecule imaging in live cells. *J. Am. Chem. Soc.* **130**, 9204–9205 (2008).
82. Gaietta, G. *et al.* Multicolor and electron microscopic imaging of connexin trafficking. *Science* **296**, 503–507 (2002).
83. Griffin, B. A., Adams, S. R. & Tsien, R. Y. Specific covalent labeling of recombinant protein molecules inside live cells. *Science* **281**, 269–272 (1998).
84. Hauser, C. T. & Tsien, R. Y. A hexahistidine-Zn^{2+}-dye label reveals STIM1 surface exposure. *Proc. Natl Acad. Sci. USA* **104**, 3693–3697 (2007).
85. Guignet, E. G., Segura, J. M., Hovius, R. & Vogel, H. Repetitive reversible labeling of proteins at polyhistidine sequences for single-molecule imaging in live cells. *Chemphyschem* **8**, 1221–1227 (2007).
86. Lata, S., Gavutis, M., Tampe, R. & Piehler, J. Specific and stable fluorescence labeling of histidine-tagged proteins for dissecting multi-protein complex formation. *J. Am. Chem. Soc.* **128**, 2365–2372 (2006).
87. Honda, K., Nakata, E., Ojida, A. & Hamachi, I. Ratiometric fluorescence detection of a tag fused protein using the dual-emission artificial molecular probe. *Chem. Commun. (Camb.)* **2006**, 4024–4026 (2006).
88. Nonaka, H., Tsukiji, S., Ojida, A. & Hamachi, I. Non-enzymatic covalent protein labeling using a reactive tag. *J. Am. Chem. Soc.* **129**, 15777–15779 (2007).
89. Ojida, A. *et al.* Oligo–Asp tag/Zn(II) complex probe as a new pair for labeling and fluorescence imaging of proteins. *J. Am. Chem. Soc.* **128**, 10452–10459 (2006).

90. McCann, C. M., Bareyre, F. M., Lichtman, J. W. & Sanes, J. R. Peptide tags for labeling membrane proteins in live cells with multiple fluorophores. *Biotechniques* **38**, 945–952 (2005).
91. Sekine-Aizawa, Y. & Huganir, R. L. Imaging of receptor trafficking by using α-bungarotoxin-binding-site-tagged receptors. *Proc. Natl Acad. Sci. USA* **101**, 17114–17119 (2004).
92. Marks, K. M., Braun, P. D. & Nolan, G. P. A general approach for chemical labeling and rapid, spatially controlled protein inactivation. *Proc. Natl Acad. Sci. USA* **101**, 9982–9987 (2004).
93. Miller, L. W., Sable, J., Goelet, P., Sheetz, M. P. & Cornish, V. W. Methotrexate conjugates: a molecular *in vivo* protein tag. *Angew. Chem. Int. Ed. Engl.* **43**, 1672–1675 (2004).
94. Miller, L. W., Cai, Y., Sheetz, M. P. & Cornish, V. W. *In vivo* protein labeling with trimethoprim conjugates: a flexible chemical tag. *Nature Methods* **2**, 255–257 (2005).
95. Gautier, A. *et al.* An engineered protein tag for multiprotein labeling in living cells. *Chem. Biol.* **15**, 128–136 (2008).
96. Keppler, A. *et al.* A general method for the covalent labeling of fusion proteins with small molecules *in vivo*. *Nature Biotech.* **21**, 86–89 (2003).
97. Keppler, A., Pick, H., Arrivoli, C., Vogel, H. & Johnsson, K. Labeling of fusion proteins with synthetic fluorophores in live cells. *Proc. Natl Acad. Sci. USA* **101**, 9955–9959 (2004).
98. Bonasio, R. *et al.* Specific and covalent labeling of a membrane protein with organic fluorochromes and quantum dots. *Proc. Natl Acad. Sci. USA* **104**, 14753–14758 (2007).
99. Los, G. V. *et al.* HaloTag: a novel protein labeling technology for cell imaging and protein analysis. *ACS Chem. Biol.* **3**, 373–382 (2008).
100. Popp, M. W., Antos, J. M., Grotenbreg, G. M., Spooner, E. & Ploegh, H. L. Sortagging: a versatile method for protein labeling. *Nature Chem. Biol.* **3**, 707–708 (2007).
101. Tanaka, T., Yamamoto, T., Tsukiji, S. & Nagamune, T. Site-specific protein modification on living cells catalyzed by Sortase. *Chembiochem* **9**, 802–807 (2008).
102. Lin, C. W. & Ting, A. Y. Transglutaminase-catalyzed site-specific conjugation of small-molecule probes to proteins *in vitro* and on the surface of living cells. *J. Am. Chem. Soc.* **128**, 4542–4543 (2006).
103. Chen, I., Howarth, M., Lin, W. & Ting, A. Y. Site-specific labeling of cell surface proteins with biophysical probes using biotin ligase. *Nature Methods* **2**, 99–104 (2005).
104. Howarth, M., Takao, K., Hayashi, Y. & Ting, A. Y. Targeting quantum dots to surface proteins in living cells with biotin ligase. *Proc. Natl Acad. Sci. USA* **102**, 7583–7588 (2005).
105. Howarth, M. *et al.* A monovalent streptavidin with a single femtomolar biotin binding site. *Nature Methods* **3**, 267–273 (2006).
106. Zhou, Z. *et al.* Genetically encoded short peptide tags for orthogonal protein labeling by Sfp and AcpS phosphopantetheinyl transferases. *ACS Chem. Biol.* **2**, 337–346 (2007).
107. Fernandez-Suarez, M. *et al.* Redirecting lipoic acid ligase for cell surface protein labeling with small-molecule probes. *Nature Biotech.* **25**, 1483–1487 (2007).
108. Baruah, H., Puthenveetil, S., Choi, Y. A., Shah, S. & Ting, A. Y. An engineered aryl azide ligase for site-specific mapping of protein–protein interactions through photo-cross-linking. *Angew. Chem. Int. Ed Engl.* **47**, 7018–7021 (2008).
109. Bossi, M. *et al.* Multicolor far-field fluorescence nanoscopy through isolated detection of distinct molecular species. *Nano. Lett.* **8**, 2463–2468 (2008).
110. Nienhaus, K., Nienhaus, G. U., Wiedenmann, J. & Nar, H. Structural basis for photo-induced protein cleavage and green-to-red conversion of fluorescent protein EosFP. *Proc. Natl Acad. Sci. USA* **102**, 9156–9159 (2005).
111. Andresen, M. *et al.* Structural basis for reversible photoswitching in Dronpa. *Proc. Natl Acad. Sci. USA* **104**, 13005–13009 (2007).
112. Chudakov, D. M., Lukyanov, S. & Lukyanov, K. A. Tracking intracellular protein movements using photoswitchable fluorescent proteins PS-CFP2 and Dendra2. *Nature Protoc.* **2**, 2024–2032 (2007).
113. Howarth, M. *et al.* Monovalent, reduced-size quantum dots for imaging receptors on living cells. *Nature Methods* **5**, 397–399 (2008).
114. Somers, R. C., Bawendi, M. G. & Nocera, D. G. CdSe nanocrystal based chem-/bio- sensors. *Chem. Soc. Rev.* **36**, 579–591 (2007).
115. Irvine, S. E., Staudt, T., Rittweger, E., Engelhardt, J. & Hell, S. W. Direct light-driven modulation of luminescence from Mn-doped ZnSe quantum dots. *Angew. Chem. Int. Ed. Engl.* **47**, 2685–2688 (2008). **Photoswitchable quantum dots developed and used for super-resolution imaging.**
116. Elmgren, H. The fluorescence lifetime of free and conjugated fluorescein in various environments. *J. Polym. Sci. [B]* **18**, 815–822 (1980).
117. Stroffekova, K., Proenza, C. & Beam, K. G. The protein-labeling reagent FLASH-EDT2 binds not only to CCXXCC motifs but also non-specifically to endogenous cysteine-rich proteins. *Pflugers Arch.* **442**, 859–866 (2001).
118. Martin, B. R., Giepmans, B. N., Adams, S. R. & Tsien, R. Y. Mammalian cell-based optimization of the biarsenical-binding tetracysteine motif for improved fluorescence and affinity. *Nature Biotech.* **23**, 1308–1314 (2005).
119. Adams, S. R. *et al.* New biarsenical ligands and tetracysteine motifs for protein labeling *in vitro* and *in vivo*: synthesis and biological applications. *J. Am. Chem. Soc.* **124**, 6063–6076 (2002).
120. Tsien, R. Y. Imagining imaging's future. *Nature Rev. Mol. Cell Biol.* **9**, S16–S21 (2003).

Acknowledgements
The authors thank X. Zhuang, E. Betzig, R.Y. Tsien, T. Uttamapinant and P. Zou for useful feedback on the manuscript.

DATABASES
UniProtKB: http://www.uniprot.org
bruchpilot | FP595 | SC35 | synaptotagmin-I | syntaxin I | TRPM5

FURTHER INFORMATION
Alice Y. Ting's homepage: http://web.mit.edu/chemistry/www/faculty/ting.html

ALL LINKS ARE ACTIVE IN THE ONLINE PDF